

IMPROVED UV NITRIDE LIGHT EMITTING DIODE WITH ENGINEERED SPONTANEOUS AND PIEZOELECTRIC CHARGES

Paul Hongen Shen, Meredith L. Reed, Eric D. Readinger and Michael Wraback
U.S. Army Research Laboratory
AMSRD-ARL-SE-EM
2800 Powder Mill Road, Adelphi, Maryland 20783

ABSTRACT

Most III-V nitride light emitting diodes have an *n*-type down structure with Ga polarity. In such a device, the active layer is grown on top of the *n*-cladding layer and the *p*-type cladding layer is grown on top of the active layer. We have analyzed the band structure of such a device and found a reduced effective conduction band barrier due to the positive spontaneous and piezoelectric polarization charge, resulting in large electron overshoot and necessitating the introduction of the commonly employed electron blocking layer. On the other hand, the polarization charge at the corresponding interface for a *p*-type down device with Ga polarity is negative, resulting in a significant enhancement of the electron barrier and the existence of a 2D hole gas near the interface. These are beneficial to the performance of single heterojunction LEDs. We have fabricated and tested such a device with a peak efficiency above 100A/cm² and only ~10% droop up to 500A/cm², which was achieved without the implementation of an AlGaN electron-blocking layer or a second hetero-interface.

1. INTRODUCTION

While many Army applications employing ultraviolet (UV) optoelectronics have been identified, including biodetection, non-line-of-sight covert communications, and water purification, logistical difficulties associated with the size, weight, cost, ruggedness, and reliability of the components has hindered system deployment. III-Nitride semiconductor ultraviolet optical sources (Nakamura, 2000, Krames, 2002) offer the possibility of compact, light-weight, low-cost, low-power-consumption optoelectronic sensors that will contribute to the sustainability of the objective force by helping in the reduction of the logistics footprint, while increasing tactical options for battlefield commanders, such as stand-off biodetection using a disposable point sensor network. In addition, biodetection, covert communication and water purification based on these devices provides protection, information, and potable water at the

individual soldier level, aiding the survivability, lethality, and deployability of the current and future force.

Typical III-Nitride semiconductor-based light emitting diodes (LED) employing multiple-quantum-well (MQW) active regions have wall plug efficiencies and lifetimes far less than those of III-V based IR LEDs. These limitations are not only due to a large density of defects caused by heteroepitaxial growth of III-Nitride based devices but also due to the strong built-in electric fields associated with spontaneous (SP) and piezoelectric (PZ) polarizations (Bykhovski, 1993, Takeuchi, 1997, Kozodov, 1999) in wurtzite structure. The electric field inside the quantum well generated by polarization charges leads to a spatial separation of electrons and holes, which lowers the probability of radiative recombination and thus lowers the emission efficiency (Park, 200). In addition to low wall plug efficiency, these devices usually exhibit further external quantum efficiency droop at high injection currents ($\geq 20\text{A/cm}^2$), which are attributed to a large electron overshoot at high injection currents resulting from the positive polarization charge near the *p*-cladding layer in a conventional *p*-up Ga-polar device (Krames, 2002). To reduce electron overshoot, an electron-blocking layer with a larger band gap must be used (Schubert, 2006). The large band gap electron blocking layer, however, increases the polarization field in the quantum well, thereby only in part ameliorating the electron leakage, while creating a potential spike in the valence band that blocks the injection of holes. Recent research (Shen, 2007) shows that the efficiency droop may relate to the strong Auger recombination in the QW and suggests that single or double heterojunction LEDs may be beneficial in achieving higher efficiency at high injection currents (Gardner, 2007). In this paper, we present both modeling and experimental results on single heterojunction LEDs and demonstrate how the negative polarization charges are beneficial by properly engineering the device layers. The benefit of such a device is the suppression of electron overshoot in combination with enhanced hole injection. Our experiments on such a device show no efficiency droop at continuous injection current densities up to 100 A/cm².

Report Documentation Page

*Form Approved
OMB No. 0704-0188*

Public reporting burden for the collection of information is estimated to average 1 hour per response, including the time for reviewing instructions, searching existing data sources, gathering and maintaining the data needed, and completing and reviewing the collection of information. Send comments regarding this burden estimate or any other aspect of this collection of information, including suggestions for reducing this burden, to Washington Headquarters Services, Directorate for Information Operations and Reports, 1215 Jefferson Davis Highway, Suite 1204, Arlington VA 22202-4302. Respondents should be aware that notwithstanding any other provision of law, no person shall be subject to a penalty for failing to comply with a collection of information if it does not display a currently valid OMB control number.

1. REPORT DATE DEC 2008	2. REPORT TYPE N/A	3. DATES COVERED -	
4. TITLE AND SUBTITLE Improved Uv Nitride Light Emitting Diode With Engineered Spontaneous And Piezoelectric Charges		5a. CONTRACT NUMBER	
		5b. GRANT NUMBER	
		5c. PROGRAM ELEMENT NUMBER	
6. AUTHOR(S)		5d. PROJECT NUMBER	
		5e. TASK NUMBER	
		5f. WORK UNIT NUMBER	
7. PERFORMING ORGANIZATION NAME(S) AND ADDRESS(ES) U.S. Army Research Laboratory AMSRD-ARL-SE-EM 2800 Powder Mill Road, Adelphi, Maryland 20783		8. PERFORMING ORGANIZATION REPORT NUMBER	
9. SPONSORING/MONITORING AGENCY NAME(S) AND ADDRESS(ES)		10. SPONSOR/MONITOR'S ACRONYM(S)	
		11. SPONSOR/MONITOR'S REPORT NUMBER(S)	
12. DISTRIBUTION/AVAILABILITY STATEMENT Approved for public release, distribution unlimited			
13. SUPPLEMENTARY NOTES See also ADM002187. Proceedings of the Army Science Conference (26th) Held in Orlando, Florida on 1-4 December 2008, The original document contains color images.			
14. ABSTRACT			
15. SUBJECT TERMS			
16. SECURITY CLASSIFICATION OF:			17. LIMITATION OF ABSTRACT
a. REPORT unclassified	b. ABSTRACT unclassified	c. THIS PAGE unclassified	UU
			18. NUMBER OF PAGES 7
			19a. NAME OF RESPONSIBLE PERSON

2. MODELING

2.1. Analytic Solution under Abrupt Approximation

Consider an n -type semiconductor with a band gap of $E_{g,n}$ and a donor concentration of N_D that forms a heterojunction with a p -type semiconductor with a band gap of $E_{g,p}$ and an acceptor concentration of N_A . At the hetero-interface, there is a sheet charge density of σ_{sp+pz} (Fig. 1). Since the electric field in the neutral regions (far from the junction) must be zero, charge neutrality requires:

$$N_D W_n + \sigma_{sp+pz} - N_A W_p = 0 \quad (1),$$

where $W_{n(p)}$ is the depletion width in the n (p) region. Under abrupt approximation, the total built-in voltage is given by

$$\frac{qN_D}{2\epsilon_n} W_n^2 + \frac{qN_A}{2\epsilon_p} W_p^2 = V_{bi,n} + V_{bi,p} = V_{bi} \quad (2),$$

where $\epsilon_{n(p)}$ is the dielectric constant for n -(p -) type material, q is the electron charge, and

$$qV_{bi} = Q_c E_{g,n} + (1 - Q_c) E_{g,p} - E_n - E_p \quad (3),$$

with Q_c the conduction band offset ratio and $E_{n(p)}$ the conduction (valence) band energy with respect to the Fermi level in the neutral region.

At $\sigma_{sp+pz}=0$, the depletion widths are

$$W_n(0) = \sqrt{\frac{2V_{bi}\epsilon_n}{qN_D}} \sqrt{\frac{1}{1+k}} \quad (4),$$

$$W_p(0) = \sqrt{\frac{2V_{bi}\epsilon_p}{qN_A}} \sqrt{\frac{k}{1+k}}$$

where $k = \frac{N_D}{N_A} \frac{\epsilon_n}{\epsilon_p}$. For $\sigma_{sp+pz} \neq 0$,

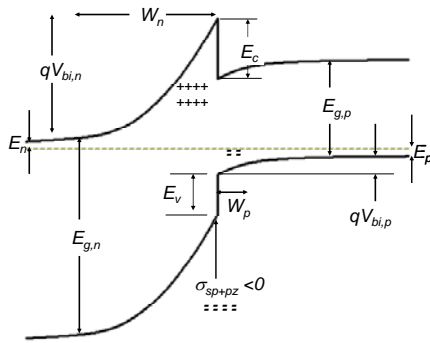


Figure 1. Illustration of band diagram for a p - n heterojunction with negative polarization charge.

$$W_n(\sigma_{sp+pz}) = W_n(0) \left[\sqrt{1 - \frac{k}{(1+k)^2} \lambda^2} - \frac{k}{1+k} \lambda \right] \quad (5),$$

$$W_p(\sigma_{sp+pz}) = W_p(0) \left[\sqrt{1 - \frac{k}{(1+k)^2} \lambda^2} + \frac{1}{1+k} \lambda \right]$$

where $\lambda = \frac{\sigma_{sp+pz}}{N_D W_n(0)} = \frac{\sigma_{sp+pz}}{N_A W_p(0)}$ is the normalized polarization sheet charge density. The band bending in the n - and p -type material is given by

$$qV_{bi,n}(\sigma_{sp+pz}) = qV_{bi} \frac{1}{1+k} \left[\sqrt{1 - \frac{k}{(1+k)^2} \lambda^2} - \frac{k}{1+k} \lambda \right]^2 \quad (6)$$

$$qV_{bi,p}(\sigma_{sp+pz}) = qV_{bi} \frac{k}{1+k} \left[\sqrt{1 - \frac{k}{(1+k)^2} \lambda^2} + \frac{1}{1+k} \lambda \right]^2$$

Figure 2 shows the normalized depletion width $W_{n,p}(\sigma_{sp+pz})/W_{n,p}(0)$ as a function of normalized polarization charge density λ at $k=1$ and 0.5 . Negative interface charge increases (decreases) the depletion width in the n -(p -) region with the band bending increasing and decreasing correspondingly. This can be understood from the charge neutrality requirement (Eq. 1) that negative interface charge requires more positive space charge from the depleted n -type layer to compensate, while positive interface charge requires more negative space charge from the depleted p -type region to compensate. However, the usable space charge in the n - and p - layer is limited and thus Eqs. 5-6 are only valid when the limitation is not reached. Since the maximum band bending is limited to the bandgap, the maximum positive (negative) space charge per unit area in an n - (p -) type material is given by

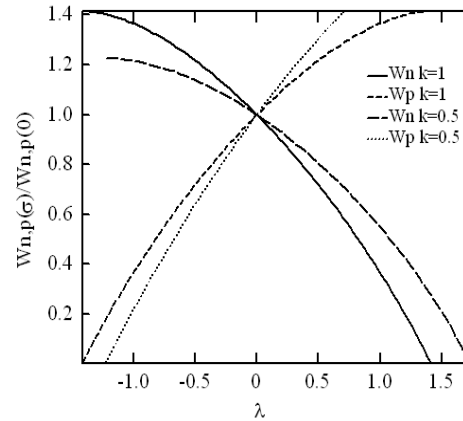


Figure 2. Normalized depletion width as a function of normalized polarization charge density.

$$\sigma_{+(-),\max} = \sqrt{\frac{2N_{D(A)}(E_{g,n(p)} - E_{n(p)})\epsilon_{n(p)}}{q}} \quad (7).$$

Figure 3 shows $\sigma_{+(-),\max}$ as a function of N_D and N_A for GaN.

In the case where $|\sigma_{sp+pz}| > \sigma_{+(-),\max}$, a 2DEG (for $\sigma_{sp+pz} > 0$) or 2DHG (for $\sigma_{sp+pz} < 0$) forms near the interface to compensate for the excess σ_{sp+pz} . The density of the 2DEG (or 2DHG) is then given by:

$$\sigma_{2DEG(2DHG)} = |\sigma_{sp+pz}| - \sigma_{+(-),\max} \quad (8).$$

It is important to point out that the 2DEG (2DHG) always appears near the hetero-interface and in the material with a smaller band gap. Therefore the conduction (valence) band offset E_c (E_v) may sometimes become involved in the calculation of maximum space charge, depending on the band gaps of the two materials. We summarize the results under various conditions in Fig. 4. We have also included the finite band bending in the 2DEG and 2DHG in the calculation. Neglecting the small difference between the Fermi level and the first confined quantum level and assuming an asymmetric triangle quantum well, we find the band bending in the 2DEG (2DHG) region as:

$$E_{2DEG(2DHG)} \approx 2.388 \left(\frac{q^2 F_{\max}^2 \hbar^2}{2m_{e(h)}} \right)^{1/3} \quad (9),$$

with F_{\max} the electric field corresponding to $\sigma_{+(-),\max}$,

$$F_{\max} = \frac{q\sigma_{+(-),\max}}{\epsilon_{n(p)}} \quad (10).$$

As an example, we consider two Ga-polar n -InGaN/ p -GaN structures, one is p -up and the other is p -down. The spontaneous and piezoelectric polarization charge (σ_{sp+pz}) at the InGaN/GaN interface is estimated to be about $1.4 \times 10^{13} \text{e/cm}^2$ and positive (negative) for p -up (p -down) Ga-polar structure. The maximum negative depletion

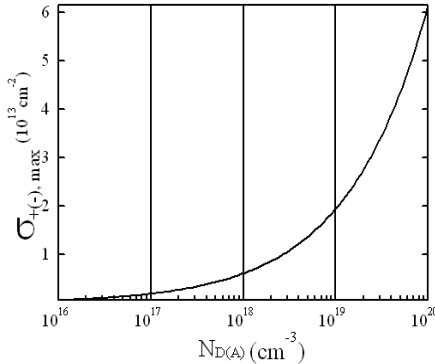


Figure 3. Maximum space charge per unit area as a function of doping concentration in GaN

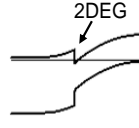
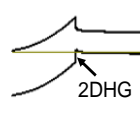
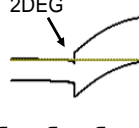
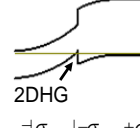
	$\sigma_{sp+pz} > 0$	$\sigma_{sp+pz} < 0$
$E_{g,n} > E_{g,p}$	 <p> $\sigma_{2DEG} = \sigma_{sp+pz} - \sigma_{-,max} + \sigma_n$ $\sigma_{-,max} = \sqrt{2N_A(E_{g,p} - E_p)\epsilon_p/q}$ $\sigma_n = \sqrt{2N_D(E_v - E_{2DEG})\epsilon_n/q}$ </p>	 <p> $\sigma_{2DHG} = \sigma_{sp+pz} - \sigma_{+,max}$ $\sigma_{+,max} = \sqrt{2N_D(E_{g,n} - E_n)\epsilon_n/q}$ </p>
$E_{g,n} < E_{g,p}$	 <p> $\sigma_{2DEG} = \sigma_{sp+pz} - \sigma_{-,max}$ $\sigma_{-,max} = \sqrt{2N_A(E_{g,p} - E_p - E_c)\epsilon_p/q}$ </p>	 <p> $\sigma_{2DHG} = \sigma_{sp+pz} - \sigma_{+,max} + \sigma_p$ $\sigma_{+,max} = \sqrt{2N_D(E_{g,n} - E_n)\epsilon_n/q}$ $\sigma_p = \sqrt{2N_A(E_v - E_{2DHG})\epsilon_n/q}$ </p>

Figure 4. 2D electron gas and 2D hole gas in various p - n heterojunctions with polarization charge larger than the maximum space charge.

charge in the p -up structure is $\sigma_{-,max} = 1.8 \times 10^{13} \text{e/cm}^2 > |\sigma_{sp+pz}|$. Therefore, there is no 2DEG in this structure. The calculated band bending in the n -type material is 20% of the total band bending (qV_{bi}), while in a similar structure without polarization charge the band bending in the n -region is $\sim 90\%$ of the total band bending. In the p -down structure, the maximum positive depletion charge is $\sigma_{+,max} = 5.7 \times 10^{12} \text{e/cm}^2 < |\sigma_{sp+pz}|$. Therefore, a 2DHG forms within the InGaN near the n -InGaN/ p -GaN interface. The calculated 2DHG density is about $1.0 \times 10^{13} \text{e/cm}^2$, which is in good agreement with the result obtained from a numerical simulation discussed below. Almost 100% of the band bending is in the conduction band.

2.2. Numerical simulation

We have modeled the p -up and p -down structure, described previously, by numerically solving the one-dimensional Poisson-Schrodinger equations self-consistently (Zhang, 1998). We define a quantum zone sandwiched between two classical zones. We have simulated the electric potential in the quantum zone and extended it continuously to a constant value outside the quantum zone. The total charge is the sum of the ionized doping charges (N_D^* , N_A^*), the free electron and hole charges (n_{free} , p_{free}), the quantum-confined electron and hole charges, and the polarization interface charge:

$$\begin{aligned} \rho(x)/q = & N_D^*(x) - N_A^*(x) - n_{free}(x) + p_{free}(x) \\ & - \sum_i n_{c,i} \psi_{c,i}^*(x) \psi_{c,i}(x) + \sum_i n_{v,i} \psi_{v,i}^*(x) \psi_{v,i}(x) n_{V,i} \\ & + \sigma_{sp+pz} \delta(x - x_0) \end{aligned} \quad (11),$$

where x_0 is the location of the hetero-interface and $n_{C(V),i}$ is the occupation of the i^{th} electron (hole) sub-band, with

its wave-function $\psi_{e(v),i}(x)$ determined by the one dimensional Schrodinger equation:

$$\frac{\hbar^2}{2} \frac{d}{dx} \left(\frac{1}{m_{e(h)}} \frac{d}{dx} \psi_{C(V),i}(x) \right) \pm (E_{C(V)}(x) - E_{C(V),i}) \psi_{C(V),i}(x) = 0 \quad (12)$$

where $E_{C(V)}(x)$ is the conduction (valence) band profile, $m_{e(h)}$ is the electron (hole) effective mass along the x direction, $E_{C(V),i}$ is the energy of the i^{th} confinement electron (hole) sub-band, and + and - signs are for electrons and holes, respectively. To distinguish quantum confined charge from free charge, a cut-off value is set at the lower potential boundary of the quantum zone. Fermi-Dirac statistics are used for free charges, while the occupation of the confined states is determined by

$$n_{C(V),i} = \frac{m_{e(h)}^{\perp} k_B T}{\pi \hbar^2} \ln \left[1 + \exp \left(\pm \frac{E_F - E_{C(V),i}}{K_B T} \right) \right] \quad (13)$$

where $m_{e(h)}^{\perp}$ is the electron (hole) in-plane effective mass, and the + and - signs are for electrons and holes, respectively.

Displayed in Fig. 5 (a) and (b) are the simulated band diagrams at zero bias for p -up and p -down structures, respectively. The parameters can be found in reference (Vurgaftman, 2003). The inset in Fig. 5(b) shows the wave-function of the first confined hole sub-band, its energy and the Fermi energy. The 2DHG density calculated from Eq. 13 is about $1.0 \times 10^{13} \text{ e/cm}^2$.

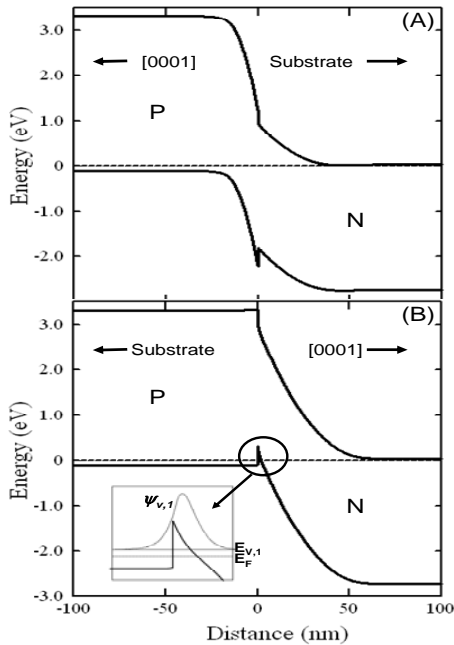


Figure 5. Band diagrams at zero bias for p -up (A) and p -down (B) devices. Inset in (B): wave-function of the first confined hole sub-band, its energy and the Fermi energy.

Figure 6 (a) and (b) show the band diagrams at a forward current density of 20 A/cm^2 for p -up and p -down devices, respectively. Poisson and drift-diffusion current equations with Fermi statistics and thermionic emission at the hetero-junction boundary are solved. The current density and the radiative recombination rate are plotted in Fig. 7 (a) and (b) for p -up and p -down devices, respectively. In the case of the p -up device, the positive polarization charge results in a substantially smaller effective electron barrier at the n -InGaN/ p -GaN interface. This leads to a significant leakage of electrons from the active n -InGaN to the p -GaN layer at room temperature (Fig. 6(a)). About 70% of the electron current overshoots into the p -GaN layer, resulting in a significant recombination within this layer (Fig. 7 (a)). In addition, the injection of holes from the p -GaN to the n -InGaN experiences a potential barrier spike up to several hundred meV, leading to very inefficient injection of holes into the n -InGaN layer (Fig. 6(a)). On the other hand, in the p -down device, the negative polarization charge at the interface leads to a substantially reduced barrier for hole injection from the p -GaN to the n -InGaN. Here, electrons encounter a significant barrier for injection from the n -InGaN into the p -GaN, making the p -GaN behave like an effective electron blocking layer (Fig. 6(b)). The formation of the 2DHG in combination with this effective electron blocking layer significantly enhances the radiative recombination of injected electrons with 2DHG in the n -InGaN active region (Fig. 7(b), dotted line).

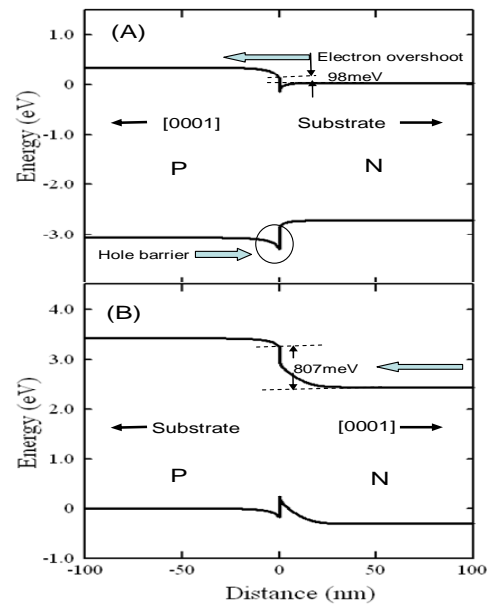


Figure 6. Band diagrams at forward current density of 20 A/cm^2 for p -up (A) and p -down (B) devices.

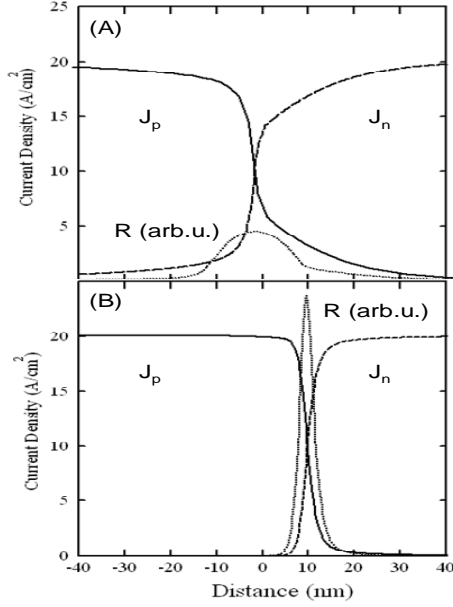


Figure 7. Current density and radiative recombination rate at forward current density of 20A/cm^2 for *p*-up (A) and *p*-down (B) devices.

To understand the recombination of electrons with the 2DHG in the *p*-down structure, we have calculated the radiative recombination rate as a function of emitted photon energy ($\hbar\nu$) using (Casey, 1969)

$$R(\hbar\nu) = 8\pi^2 B \sum_{i_{\text{hole}}} dE dk_{\perp} 2\pi k_{\perp} f(E - E_{f,c}) * f(E_{f,v} - E + \hbar\nu) M^2(i_{\text{hole}} E - \frac{\hbar^2 k_{\perp}^2}{2m_e^{\perp}}) \quad (14)$$

where B contains the average inter-band matrix element that is assumed independent of the initial and the final states, E is the total electron energy, $E_{f,c(v)}$ is the quasi Fermi energy for the electron (hole), $f(E')$ s are the Fermi distribution functions for electrons and holes, $\hbar k_{\perp}$ is the in-plane momentum, and M is the overlap integral between the electron and confined hole wave-functions:

$$M(i, E) = \int dx \psi_c(E) \psi_{v,i} \quad (15)$$

Figure 8 shows R as a function of photon energy at various injection current densities. At low injection current density, the peak emission energy shifts to higher energy with a corresponding superlinear increase in light output (Fig. 8, inset) as the injection current increases. At higher injection currents, a linear increase in intensity is reached with slower blue shift in peak energy. Also noted is that the emission intensity at energies lower than the peak energy shows saturation, while the emission

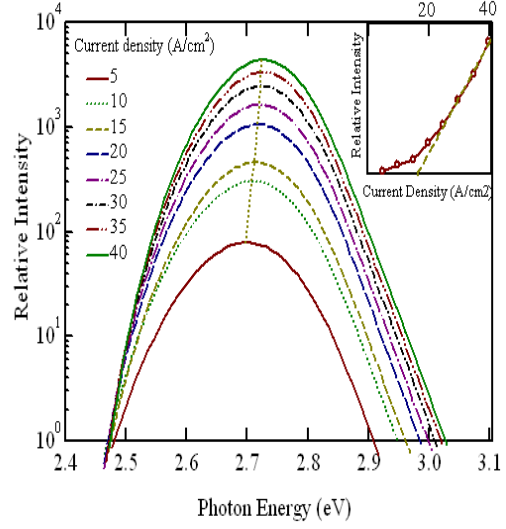


Figure 8. Radiative recombination as a function of photon energy at various injection current densities. Inset shows light output as a function of injection current density.

intensity at higher energies increases rapidly without saturation. The physics of the shifting-peak spectra is similar to that of photo-assisted tunneling reported in GaAs *p-n* junctions (Casey, 1969), except that the hole states here are confined. Under forward bias, some of the injected electrons undergo spatially indirect recombination with the 2DHG. With increasing forward bias, the electron quasi-Fermi level increases, leading to more high energy electrons recombining with the 2DHG and a concomitant blue shift of the electroluminescence. This effect, in combination with the improved overlap of electron and hole wave-functions, leads to a superlinear increase in light output.

3. EXPERIMENTAL RESULTS

Single heterojunction (SH) *n*-InGa_N/*p*-Ga_N structures with *p*-type down (*p*-down) are grown on an *n*-Ga_N template by HVPE on a sapphire substrate. Mesas are defined using standard RIE-ICP etching with an etch depth of $0.5\ \mu\text{m}$ to contact the *p*-Ga_N. Ni/Au *p*-contacts are e-beam evaporated and annealed at $650\ \text{°C}$ for 2 minutes in N_2 . Indium tin oxide (ITO) *n*-contacts are RF sputtered as the final step in the process. Wafer level I-V and transmission line measurements (TLM) are performed on the SH LEDs. Details of the device processing may be found elsewhere (Reed, 2007). Devices are packaged and electroluminescence measurements are performed using an integrating sphere and an Ocean Optics spectrometer. Figure 9 shows the typical emission spectrum at 10% duty cycle at different currents for the *n*-InGa_N/*p*-Ga_N *p*-down

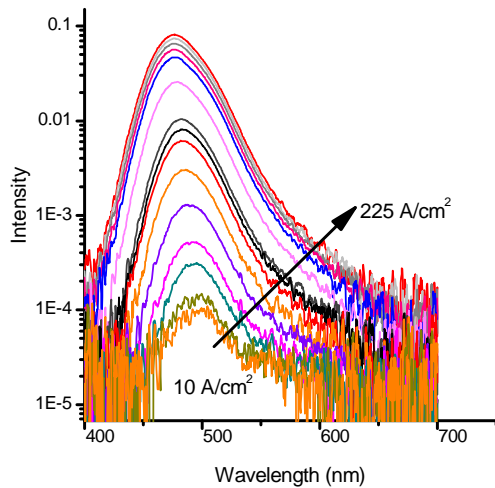


Figure 9. Typical emission spectra at 10% duty cycle (DC) current densities for the *n*-InGaN/*p*-GaN *p*-side down, Ga-polar devices having 22% indium composition at various injection current densities.

Ga-polar devices. The normalized peak intensity and the percentage blue shift of the peak wavelength as a function of current density are shown in figure 10. The peak emission wavelength blue shifts with a simultaneous superlinear increase in light output as the injection current increases from 8–40 A/cm². At higher injection currents a linear increase in intensity is observed with no further blue shift in peak wavelength. These behaviors are in good agreement with our modeling. For 1% DC, the peak EQE is attained above 100 A/cm², with only about 10%

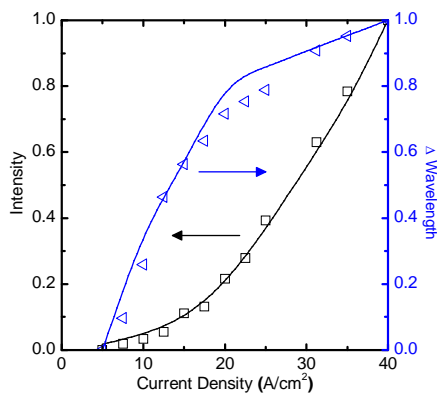


Figure 10. Percentage change in peak wavelength shift and normalized output power at low current density, for both predicted (solid line) and measured device behavior (data points). The data shows good agreement with our predicted model.

droop up to 500 A/cm². Devices of different In content show qualitatively similar behavior. The fact that the emission intensity increases linearly from 20 A/cm² to 40 A/cm² without saturation implies a relatively constant external quantum efficiency at significantly higher injection current densities than reported for MQW devices operating at comparable wavelengths (Gardner, 2007).

CONCLUSIONS

We have analyzed the effects of polarization charge on single heterojunction LEDs. Positive polarization charge in a conventional *p*-up structure is detrimental. It lowers the effective conduction barrier for electrons, leading to large electron overshoot, and at the same time increases the potential barrier for holes, reducing hole injection. Negative polarization charge in a *p*-down structure is beneficial. It significantly enhances the electron barrier and lowers the hole barrier, creating an associated 2DHG and leading to an overall improvement in the injection efficiency. The lack of significant efficiency droop in our devices at pulsed current densities up to 500A/cm² shows promise for high current density applications.

REFERENCES

- Nakamura, S. and Fasol, G., 2000, *The Blue Laser Diode*, Springer, Berlin.
- Krames, M.R., Bhat, J., Collins, D., Gardner, N.F., Göetz, W., Lowery, C. H., Ludowise, M., Martin, P.S., Mueller, G., Mueller-Mach, R., Rudaz, S., Steigerwald, D.A., Stockman, S.A., and Wierer, J. J., 2002, High-Power III-Nitride Emitters for Solid-State Lighting *Physica Status Solidi (a)*, 192(2), 237.
- Bykhovski, A., Gelmont, B., and Shur, M., 1993, The influence of the strain-induced electric field on the charge distribution in GaN-AlN-GaN structure, *J. Appl. Phys.* 74, 6734.
- Takeuchi, T., Sota, S., Katsuragawa, M., Komori, M., Takeuchi, H., Amano, H., and Akasaki, I., 1997, Quantum-Confined Stark Effect due to Piezoelectric Fields in GaInN Strained Quantum Wells, *Jpn. J. Appl. Phys.*, Part 2, 36, L382.
- Kozodov, P., Hansen, M., DenBaars, S. P., and Mishra, U. K., 1999, Enhanced Mg doping efficiency in Al_{0.2}Ga_{0.8}N/GaN superlattices, *Appl. Phys. Lett.* 74, 3681.
- Ibbetson, J. P., Fini, P. T., Ness, K. D., DenBaars, S. P., Speck, J. S., and Mishra, U. K., 2000, Polarization effects, surface states, and the source of electrons in AlGaIn/GaN heterostructure field effect transistors, *Appl. Phys. Letts.* 77, 250.
- Park, S-H. and Chuang, S-L, 2000, Spontaneous polarization effects in wurtzite GaN/AlGaIn quantum wells and comparison with experiment, *Appl. Phys. Letts.* 76, 1981.

- Schubert, E. F., 2006, *Light-Emitting Diodes*, p82, Cambridge, New York.
- Shen, Y. C., Mueller, G. O., Watanabe, S., Gardner, N. F., Munkholm, A., and Krames, M. R., 2007, Auger recombination in InGaN measured by photoluminescence, *Appl. Phys. Lett.* 91, 141101.
- Gardner, N. F., Mueller, G. O., Shen, Y. C., Chen, G., Watanabe, S., Goetz, W., and Krames, M. R., 2007, Blue-emitting InGaN–GaN double-heterostructure light-emitting diodes reaching maximum quantum efficiency above 200 A/cm² *Appl. Phys. Lett.* 91, 243506.
- Zhang Y., and Singh, J., 1998, Charge control and mobility studies for an AlGaN/GaN high electron mobility transistor, *J. Appl. Phys.* 85, 587.
- Vurgaftman, I. and Meyer, 2003, Band parameters for nitrogen-containing semiconductors, *J. Appl. Phys. Rev.* 94, 3675.
- Casey, H. C. and Silversmith, D. J., 1969, Radiative Tunneling in GaAs Abrupt Asymmetrical Junctions, *J. Appl. Phys.* 40, 241.
- Reed, M. L., Readinger, E. D., Shen, P., and Wraback, M., Syrkin, A., Usikov, A., and Dmitriev, V., 2007, Device Challenges for Making a p-Side Down HVPE-Grown n-InGaN/p-GaN Single Heterostructure LED, *Electrochem. Soc. Tran* 11(5) 171-174.